JOURNAL OF PROPULSION AND POWER
Vol. 8, No. 3, May–June 1992

Turbomachinery Unsteady Load Predictions with Nonuniform Inflow

Shih H. Chen*
Rockwell International Corporation, Canoga Park, California 91303

A two-dimensional frequency domain source-doublet based potential paneling formulation is developed to predict steady and unsteady turbomachinery blade loadings. The method employed blade-to-blade periodic boundary condition and interblade phase angles to simulate the complex blade-wake interactions in turbomachinery stages. The method is used in the present paper to simulate the unsteady response on Space Shuttle main engine high-pressure oxidizer turbopump diffuser blades. The amplitude of unsteady pressure and the wave propagation characteristics are discussed by comparing similar studies.

Nomenclature

B_{ij} = blade source influence coefficient
C_{ij} = blade doublet influence coefficient
C_p = pressure coefficient
G = Green's function
k = wake element index
l = blade index
m = harmonics index
NT = current time step
n = surface outward unit normal
nb_1 = number of blade on 1st row
nb_2 = number of blade on 2nd row
p = pressure
R = distance between any two points in space
S = surface of body
T = period of disturbing wave
t = reference time
U = velocity
U_m = far upstream mean x-component velocity
V_m = far upstream mean y-component velocity
v_n = surface normal velocity
W_{iw} = wake doublet influence coefficient
x = x coordinate
y = y coordinate
Δt = time step
Δu_x = x-component unsteady velocity
Δu_y = y-component unsteady velocity
Δy_1 = pitch of 1st row
Δy_2 = pitch of 2nd row
$\Delta\theta_x$ = phase angle of Δu_x
$\Delta\theta_y$ = phase angle of Δu_y
$\Delta\varphi$ = inter-wake element phase lag
ρ = density
σ = interblade phase angles
τ = retarded time
ϕ = perturbation velocity potential
ω = excitation frequency
ω_o = fundamental excitation frequency

Subscripts
0 = reference blade
∞ = property at infinity
j = panel index
l = lower surface
m = mean value
st = steady state
TE = trailing edge
u = upper surface
un = unsteady part
w = wake
x = x-component
y = y-component
$-$ = mean value
$\sim$ = unsteady fluctuation amplitude

Introduction

IT is well known that the flow structure in a turbomachinery passage is extremely complex, especially in the compressor or turbine stages. For this reason, the majority of turbomachinery blade aerodynamic analysis is steady state. This is based on the assumption that the rotor and stator are far apart, that the flow in each is steady, and that interactions between blade rows are negligible. In reality, the gaps between blade rows are generally 20–50% of a chord length and the interactions between blade rows are generally not small. The wakes shed by the upstream blade or vane rows are not uniform, due to viscous effects and interactions with the downstream blades (Fig. 1). The unsteady wake is considered to be the most common aerodynamic excitation source to the downstream blades. The unsteady force produced by the wake can cause turbomachinery blade high-cycle fatigue failures. Specific components that had encountered unex-

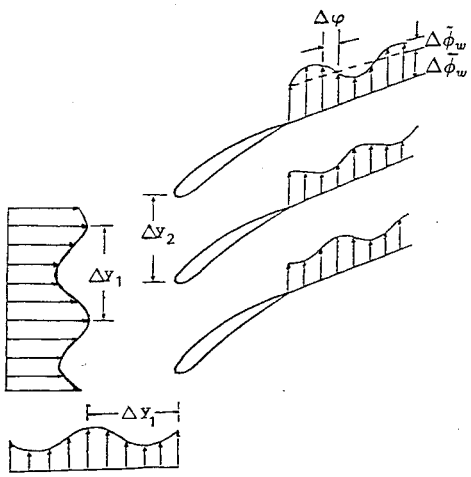

Fig. 1 Gust and unsteady wake model.

Presented as Paper 89-0450 at the AIAA 27th Aerospace Sciences Meeting, Reno, NV, Jan. 9–12, 1989; received March 13, 1990; revision received May 24, 1991; accepted for publication July 17, 1991.

*Member of Technical Staff, Rocketdyne Division. Member AIAA.

pected blade cracking are certain turbomachinery blades in the Space Shuttle main engine (SSME) turbopumps.

Frequently, the structural dynamic analysis of turbomachinery blading consists of simply calculating the natural frequencies and avoiding known forcing functions. Forced response calculations are not attempted. Due to the increasing concern about turbomachine blade cracks during development or operation, the understanding of the blade response to nonuniform upstream disturbances becomes very important. Smith[1] developed a linear analysis for thin turbomachinery blades by assuming a sinusoidal upstream disturbance that is perpendicular to the blade chord. He modeled the cascade blades with a finite number of fixed vortices. Instead of applying vortex methods to the modeling of cascade blades, Fleeter[2] solved the two-dimensional partial differential equation that describes the perturbation velocity potential through the application of Fourier transform theory. Henderson's work[3] is based on a similar approach but includes small camber, thickness, and incidence to the cascade with the assumption that the wavelength of the distorted inflow is much larger than blade spacing. These approaches are not suitable for cascades with large camber, thickness, and incidence in a high-frequency disturbance flowfield. With the advent of high-speed computers and progress in calculating differential equations, the simulation of unsteady flow on real turbomachinery configurations is possible. Notable efforts to develop computational methods to describe adequately the complicated flow around interacting blade rows include solving a coupled rotor-stator in an unsteady frame,[4–6] and solving a circumferential averaged multistage turbomachinery passage flow.[7] However, all of the attempts require tremendous amounts of computer time and are not efficient for design purposes.

The need for an efficient method to predict the forced response of turbomachinery blades to a time-dependent excitation has led to the development of the unsteady analysis for a turbomachinery blade cascade with thickness and camber in a high-frequency environment. A theory similar to Morino's, Green's function paneling method,[8] is used. A code for frequency domain analysis is also developed. A Fourier analysis is incorporated with the frequency domain analysis to model better the incoming distorted flow. An unsteady wake model with phase difference between wake segments is adopted. In addition, interblade phase angles, which depend on the number of blades and disturbing wave length between blades and wakes, are used. This method had been applied to various turbomachinery cascade flows with good agreement with measurements in both steady and unsteady calculations.[9,10] In the present paper, this method is used to simulate the unsteady loads on SSME High Pressure Oxidizer Turbopump (HPOTP) diffuser blades where both upstream velocity[11] and limited surface dynamic pressure measurements[12] are available for comparison. The amplitude of pressure fluctuations and wave propagation characteristics are discussed.

Theory

Assuming the flow past a body in space is incompressible, irrotational, and inviscid, the governing equation is Laplace's equation

$$\nabla^2\phi = 0 \tag{1}$$

where ϕ is perturbation velocity potential. Using Green's theorem, the potential field at any instant in time, and any field point x, can be expressed as a distribution of source and doublet over the boundary surface S, which includes all the blades and their wakes

$$E\phi(x, t) = \int \frac{\partial \phi}{\partial n} G \, ds - \int \frac{\partial G}{\partial n} \phi \, ds \tag{2}$$

where

$$G = \frac{\ell_n R}{2\pi} = \text{Green's function in two dimensions}$$

$$R = |x - x_o| = \text{distance between any two points.}$$

Eq. (2) can then be expressed as

$$2\pi E\phi(x, t) = \int \frac{\partial \phi}{\partial n} \ell_n R \, ds - \int \phi \frac{\partial}{\partial n} (\ell_n R) \, ds \tag{3}$$

where

$$E = 0 \text{ inside } S$$
$$= 1/2 \text{ on } S$$
$$= 1 \text{ outside } S$$

The first term on the right-hand side of Eq. (3) represents the source distribution, which is known from the flow tangency boundary condition on solid surfaces. The second term on the right-hand side represents the unknown doublet distribution. When specialized to the blade surfaces, Eq. (3) amounts to a Fredholm integral equation of the second kind, which must be solved for the potential distribution on the surface.

Discretization

In order to obtain a numerical solution for the integral Eq. (3), it is necessary to approximate the curved body and wake surfaces by a large number of small elements, Fig. 2. Each element is a linear line segment with the surface normal n pointing outward from the surface to the fluid.

If the body in consideration is a blade row and the blades are assumed to be identical to each other within each row, only one blade (the reference blade) geometry need be specified. The other blade coordinates are decided by the reference blade with relative x and y spacings. Δx_d and Δy_d

$$\begin{aligned} P_{xi} &= P_{xoi} \pm \Delta x_d(l - 1) \\ P_{yi} &= P_{yoi} \pm \Delta y_d(l - 1) \end{aligned} \tag{4}$$

The $\pm$ sign is decided by the relative position of blades to the reference blade.

One control point for each surface panel is used. The choice of the panel centroid as the control point is believed to give the most satisfactory results. Piecewise constant singularity distribution over each panel surface is assumed, that is ϕ_j, $(\partial\phi/\partial n)_j$ = constant. Eq. (3) can be represented by

$$\phi_i = \frac{1}{\pi} \sum_l \sum_j \frac{\partial \phi(l, j)}{\partial n} \int \ell_n R \, ds - \frac{1}{\pi} \sum_l \sum_j \phi(l, j) \cdot \int \frac{\partial}{\partial n} \ell_n R \, ds - \frac{1}{\pi} \sum_l \sum_k \Delta\phi_w(l, k) \int \frac{\partial}{\partial n_w} \ell_n R \, ds_w \tag{5}$$

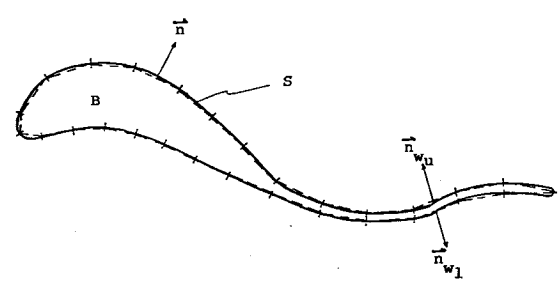

Fig. 2 Blade and wake surface paneling.

The $\boldsymbol{n}_w$ directs to the wake upper surface with $\boldsymbol{n}_w = \boldsymbol{n}_{w_u} = -\boldsymbol{n}_{w_l}$ and wake doublet $\Delta\phi_w = \phi_{w_u} - \phi_{w_l}$. Note that the source term disappeared for the wake integral because the wake is of infinitesimal thickness.

Wake Modeling

The wake is assumed to be infinitesimally thin, emanating from the blade trailing edge and convected downstream with the axial velocity component equal to the mean freestream axial velocity. The wake strength is a function of vorticity and is varying periodically with the same frequency as the upstream disturbance (see Fig. 1). There is a phase lag $\Delta\varphi$ between neighboring wake panels. The phase is decided by the disturbing wavelength and the time step used to describe wake elements, i.e.

$$\Delta\varphi = 2\pi \frac{\Delta t}{T} = \omega_o m \Delta t \tag{6}$$

We can then express the entire unsteady wake doublet strength in terms of wake doublet strength on the wake panel next to the trailing edge

$$\Delta\tilde{\phi}_w(l, k) = (\Delta\tilde{\phi}_{w_{TE}}(l))e^{-i(NT-k)\Delta\varphi} \tag{7}$$

where NT denotes current time step and k denotes any time step at which the wake elements were generated.

The wake doublet strength near the trailing edge is determined by the blade doublet strength at the trailing edge from the numerical Kutta condition. The Kutta condition is satisfied by assuming equal pressure across the trailing edge of the blade. This is represented numerically from the unsteady Bernoulli's equation by

$$\Delta\tilde{\phi}_{w_{TE}}(l) = (\tilde{\phi}_{w_u}(l) - \tilde{\phi}_{w_l}(l)) = (1 - im\omega_o\Delta t)(\Delta\tilde{\phi}_{TE}) \tag{8}$$

for unsteady conditions, and

$$\Delta\tilde{\phi}_w = \Delta\tilde{\phi}_{TE} = \tilde{\phi}_{TE_u} - \tilde{\phi}_{TE_l} \tag{9}$$

for steady state conditions.

Interblade Phase Angle

The blades are assumed rigid and identical. The loading on blades is periodic with a phase angle σ between neighboring blades at identical chordwise location. If nb is the number of blades in a row and N is the number of gust periodic distortions per revolution, then the magnitude of the interblade phase angle in radians is the circumferential arc divided by the number of blades per wave:

$$\sigma = \frac{2\pi N}{nb} \tag{10}$$

If we express the phase angle in terms of pitches Δy_1 and Δy_2, Eq. (10) can be written as

$$\sigma = 2\pi \frac{\Delta y_2}{\Delta y_1} \tag{11}$$

or

$$\sigma = 2\pi \frac{nb_1}{nb_2} \tag{12}$$

where nb_1 is a fictitious upstream blade number and nb_2 is a downstream blade number. For higher frequencies based on a given fictitious blade number, we may also write Eq. (12) in a more general form

$$\sigma = 2\pi m \frac{nb_1}{nb_2} \tag{13}$$

where $m = 1 - M$ = harmonic index. Thus, the second term on the right-hand side of Eq. (5) can be written in terms of the interblade phase angle as

$$\begin{aligned}\frac{1}{\pi}\sum_l \sum_j \phi(l, j) \int \frac{\partial}{\partial n}(\ell_n R)\, ds &= \frac{1}{\pi}\sum_j \left[\tilde{\phi}_j \sum_l \left(\int \frac{\partial}{\partial n}(\ell_n R)\, ds\right)\right] \\ &+ \frac{e^{im\omega_o t}}{\pi}\sum_j \left\{\tilde{\phi}_{jo} \sum_l \left[(e^{\pm i(l-1)\sigma}) \int \frac{\partial}{\partial n}(\ell_n R) ds\right]\right\}\end{aligned} \tag{14}$$

where subscript o of ϕ denotes the reference blade.

Because the wake doublet strength depends on the blade surface doublet strength, and the blade surface doublet is blade-to-blade periodic with a phase angle σ, the wake doublet is also blade-to-blade periodic with the same phase angle σ. Thus, the last term on the right hand side of Eq. (5) yields

$$\begin{aligned}\frac{1}{\pi}\sum_l \sum_k \Delta\phi_w(l, k) \int \frac{\partial}{\partial n_w}(\ell_n R)\, ds_w &= \frac{1}{\pi}\Delta\tilde{\phi}_w \sum_l \sum_k \\ &\cdot \int \frac{\partial}{\partial n_w}(\ell_n R)\, ds_w + \frac{e^{im\omega_o t}}{\pi}\Delta\tilde{\phi}w_{TE_o} \sum_l e^{\pm i(l-1)\sigma} \\ &\cdot \sum_k (e^{-i(NT-k)\Delta\varphi}) \int \frac{\partial}{\partial n_w} \ell_n R\, ds_w\end{aligned} \tag{15}$$

Blade Boundary Condition

As we assume the blades are rigid, the self-induced unsteady aerodynamic forces generated when the blade row responds to the aerodynamic forcing function are not considered here. The boundary condition on the blade surfaces is the standard solid wall nonpenetrating condition. The normal velocity on the surface is

$$v_n(l, j) = -\boldsymbol{U} \cdot \boldsymbol{n} \tag{16}$$

where $\boldsymbol{n}$ is the surface outward unit normal points to the fluid, and $\boldsymbol{U}$ is the time dependent freestream velocity.

In the frequency domain unsteady analysis, we do not trace the in-passage deformed vortical flow in a time marching manner. Instead, we adopted a linear gust convection model similar to the one used by Fleeter,[2] in which the unsteady disturbances travel with the flow at a speed equaling the axial mean flow. This assumption should be good[10] as long as there is no significant flow distortion or flow separation on the blade surface. Thus, the flow felt by a point $\boldsymbol{x}$ on the blade surface at time t is as if the flow was generated at the inlet of the cascade at an earlier time τ

$$\begin{aligned}\boldsymbol{U}(\boldsymbol{x}, t) &= [U_m + \Delta u_x e^{i(\Delta\theta_x + m\omega_0\tau \pm (l-1)\sigma)}]\boldsymbol{i} \\ &+ [V_m + \Delta u_y e^{i(\Delta\theta_y + m\omega_0\tau \pm (l-1)\sigma)}]\boldsymbol{j}\end{aligned} \tag{17}$$

where τ equals $t - x_j/U_m$, and σ is the interblade phase angle.

The normal velocity in Eq. (16) can be expressed as

$$\begin{aligned}v_n(l, j) = -[U_m + \Delta u_x e^{i(\Delta\theta_x + m\omega_0\tau \pm (l-1)\sigma)}]n_{x_j} - [V_m \\ + \Delta u_y e^{i(\Delta\theta_y + m\omega_0\tau \pm (l-1)\sigma)}]n_{y_j} = \bar{v}_n(j) + \tilde{v}_n(l, j)e^{im\omega_o t}\end{aligned} \tag{18}$$

where $\bar{v}_n$ is the steady normal velocity

$$\bar{v}_{n_j} = \bar{v}_n(j) = -U_m n_{x_j} - V_m n_{y_j} \tag{19}$$

and $\tilde{v}_n$ is the unsteady normal velocity

$$\tilde{v}_n(l, j) = \tilde{v}_{n_{jo}} e^{\pm i(l-1)\sigma} = \Delta u_x e^{i(\Delta\theta_x - m\omega_o x_j/U_m \pm (l-1)\sigma)} n_{x_j} + \Delta u_y e^{i(\Delta\theta_y - m\omega_o x_j/U_m \pm (l-1)\sigma)} n_{y_j} \quad (20)$$

The source term in Eq. (5) can, thus, be written as

$$\frac{1}{\pi}\sum_l \sum_j \frac{\partial \phi(l, j)}{\partial n} \int \ell_n R \, ds = \frac{1}{\pi}\sum_j \left[\tilde{v}_{n_j} \sum_l \int \ell_n R \, ds\right] + \frac{e^{im\omega_o t}}{\pi}\sum_j \left[\tilde{v}_{n_{jo}} \sum_l e^{\pm i(l-1)\sigma} \int \ell_n R \, ds\right] \quad (21)$$

Solution for Velocity Potential

Combining Eqs. (5), (14), (15), and (21) yields

$$[\delta_{ij} - \bar{C}_{ij}]\{\bar{\phi}_j\} - [\bar{W}_{iw}]\{\Delta\bar{\phi}_w\} + [\delta_{ij} - \tilde{c}_{ij}]\{\tilde{\phi}_{jo}\} - [\tilde{w}_{iw}]\{\Delta\tilde{\phi}_{wo}\} = [\bar{B}_{ij}]\{\bar{v}_{nj}\} + [\tilde{b}_{ij}]\{\tilde{v}_{njo}\} \quad (22)$$

where

δ_{ij} = Kronecker Delta function

$$\bar{C}_{ij} = \frac{-1}{\pi}\sum_l \int \frac{\partial}{\partial n} \ell_n R \, ds$$

$$\tilde{c}_{ij} = \frac{-e^{im\omega_o t}}{\pi}\sum_l (e^{\pm i(l-1)\sigma}) \int \frac{\partial}{\partial n} \ell_n R \, ds$$

$$\bar{W}_{iw} = \frac{-1}{\pi}\sum_l \sum_k \int \frac{\partial}{\partial n_w} \ell_n R \, ds_w$$

$$\tilde{w}_{iw} = \frac{-e^{im\omega_o t}}{\pi}\sum_l e^{\pm i(l-1)\sigma} \sum_k e^{-i(NT-k)\Delta\varphi} \int \frac{\partial}{\partial n_w} \ell_n R \, ds_w$$

$$\bar{B}_{ij} = \frac{1}{\pi}\sum_l \int \ell_n R \, ds$$

$$\tilde{b}_{ij} = \frac{e^{im\omega_o t}}{\pi}\sum_l e^{\pm i(l-1)\sigma} \int \ell_n R \, ds$$

The steady part and unsteady part in Eq. (22) can be considered separately, that is

$$[\delta_{ij} - \bar{C}_{ij}]\{\bar{\phi}_j\} - [\bar{W}_{iw}]\{\Delta\bar{\phi}_w\} = [\bar{B}_{ij}]\{\bar{v}_{nj}\} \quad (23)$$

$$[\delta_{ij} - \tilde{c}_{ij}]\{\tilde{\phi}_{jo}\} - [\tilde{w}_{iw}]\{\Delta\tilde{\phi}_{wo}\} = [\tilde{b}_{ij}]\{\tilde{v}_{njo}\} \quad (24)$$

For the steady part, Eq. (23) gives the steady solution, $\bar{\phi}_j$; and for the unsteady part, Eq. (24) gives the unsteady solution $\tilde{\phi}_{jo}$.

Pressure Calculation

The pressure is calculated using the unsteady Bernoulli's equation once the velocity potential is obtained

$$\frac{p'}{\rho} = -\frac{\partial\phi}{\partial t} - \boldsymbol{U}\cdot\nabla\phi - \frac{1}{2}|\nabla\phi|^2 \quad (25)$$

and the pressure coefficient is the pressure normalized by the inlet mean dynamic head

$$C_p = \frac{p'}{\frac{1}{2}\rho U_\infty^2} = \frac{p - p_\infty}{\frac{1}{2}\rho U_\infty^2} \quad (26)$$

The fluctuating part of the unsteady pressure is obtained by subtracting the steady state solution, i.e.

$$dC_p(m) = C_{p_{un}}(m) - C_{p_{st}} \quad (27)$$

Overall pressure is a summation of all steady and unsteady pressures

$$C_{pT} = C_{p_{st}} + \sum_m dC_p(m) e^{i\omega_0 mt} \quad (28)$$

High-Pressure Oxidizer Turbopump (HPOTP) Diffuser Blade

The steady and unsteady pressure on a modified high-pressure oxidizer turbopump (HPOTP) diffuser configuration of the Space Shuttle main Engine (SSME) was studied experimentally in a water test by Arndt et al.[13] In their study, the vane pressure fluctuation characteristics were found to be somewhat different from those of typical axial flow thin trailing edge cascades. The interactions between impeller and diffuser blades are characterized by the flow coefficients and the gap between two blade rows.

The current analysis on HPOTP diffuser blades utilizes a velocity measurement in an air test (see Ref. 11). Hot wire anemometer measurements were made of the radial and tangential velocity components U_r and U_θ between the impeller exit and diffuser inlet. The HPOTP centrifugal impeller consists of four full blades and four partial blades. The four full blades are assumed identical and the four partial blades are identical. Thus, the fundamental blade passing period is defined as the time for the impeller to rotate 90 degs. Fig. 3 shows the measured velocities for one 360 deg of blade rotation at a rotating speed of 14,500 rpm. The diffuser blades are composed of 15 equally spaced identical blades with high stagger angle. The coordinate of the diffuser blades and measured velocities were log-spiral transformed to a Cartesian coordinate. The radial velocity U_r becomes axial velocity U_x and the tangential velocity U_θ becomes U_y.

The transformed velocity fields are Fourier decomposed into many harmonics with magnitudes Δu_x, Δu_y and phases $\Delta\theta_x$, $\Delta\theta_y$. The discrete frequencies correspond to the blade passing frequency and its multiples. The first four frequencies were picked for the present calculation.

With the unsteady velocities and their phase angles, the surface normal velocity can be calculated from Eq. (18). The steady and unsteady solution for velocity potential are obtained from Eqs. (23) and (24). The pressure distributions for each individual frequency are calculated and the summation over the four harmonics is shown in the next section.

Results and Discussion

In this section both the results for HPOTP diffuser blades in the frequency frame and time dependent frame are presented. Figure 4 shows the mean (the solid line), and the maximum/minimum pressures (the dashed line) along the surface throughout the entire history. The mean loading decays along the chord while the unsteady part variation does not

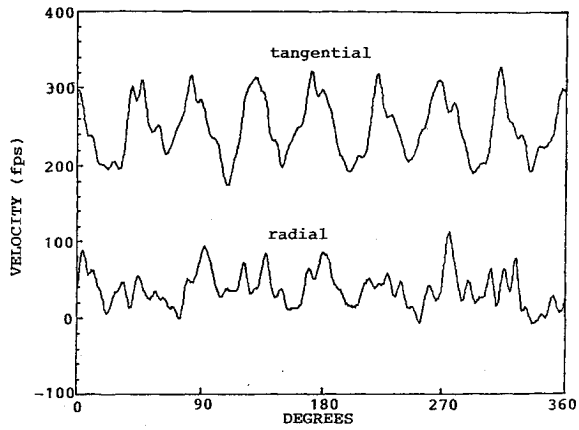

Fig. 3 Unsteady wake velocity.

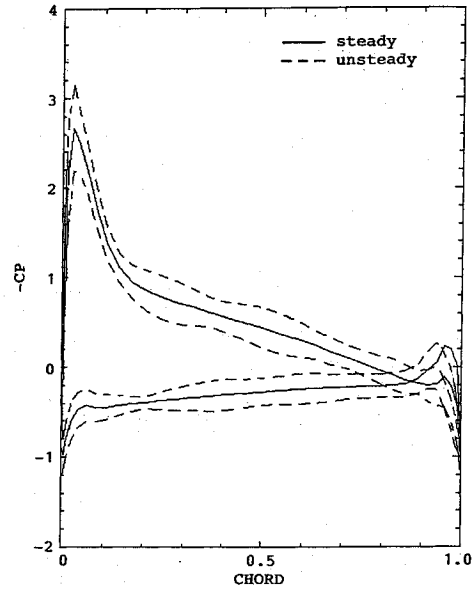

Fig. 4 Steady and unsteady loading.

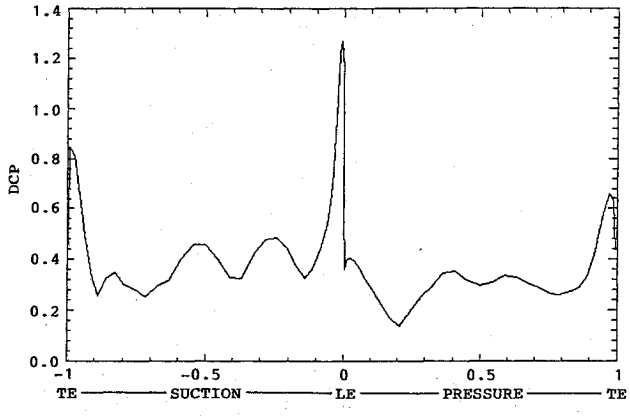

Fig. 5 Amplitude of pressure fluctuation.

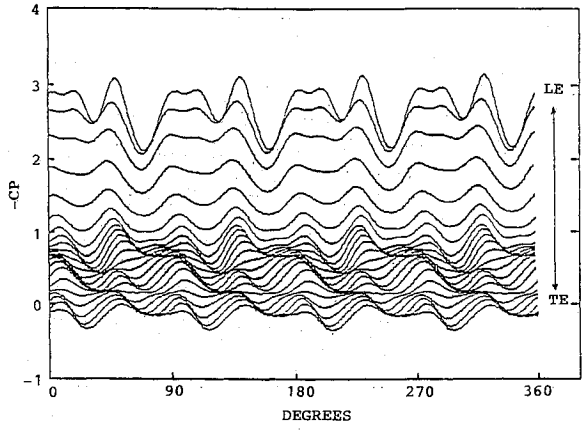

Fig. 6 Suction surface loading history.

decay monotonically along the chord. Wavy forms of unsteady pressure fluctuations were observed on both surfaces. This type of response resemble those obtained by Rai,[4] Chen,[6] and Dring et al.[14] for stator-rotor interaction studies. The largest peak-to-peak pressure fluctuation was observed near the leading edge on the suction surface, Fig. 5, with an amplitude larger than the mean inlet velocity head. It implies that this region near the leading edge on the suction surface suffers mostly due to the nonuniformity of the flowfield. This excessive dynamic loading at the leading edge is a possible cause

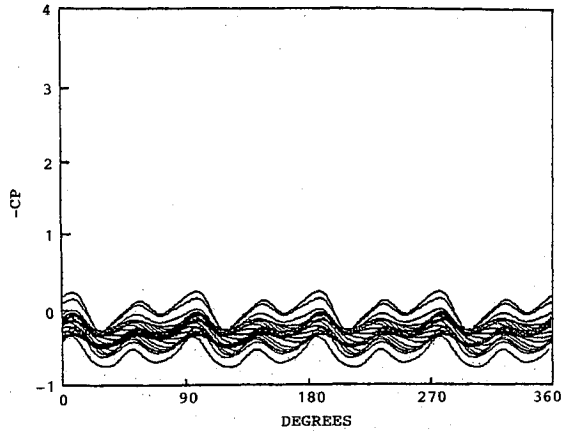

Fig. 7 Pressure surface loading history.

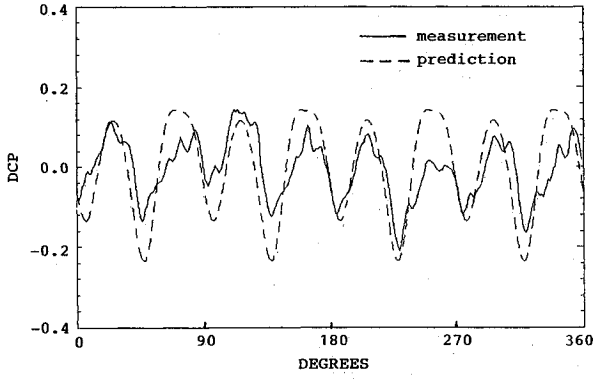

Fig. 8 Comparison of predicted and measured diffuser blade unsteady pressure (suction side).

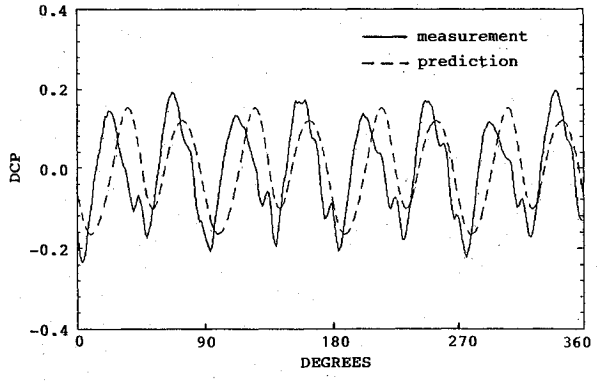

Fig. 9 Comparison of predicted and measured diffuser blade unsteady pressure (pressure side).

of most turbomachinery blade leading edge cracks. Moreover, the response near the trailing edge is also found to be large, which agrees with the observation shown by Arndt et al.[13] The not so small unsteady pressure at the trailing edge differs from those of typical compressor cascades. This could be due both to the thick trailing edge and high loading on the blades. Generally speaking, the pressure fluctuations on the suction side are larger than those on the pressure side.

An alternative view of the pressure fluctuations is to expand the loading into a time frame for one 360-deg impeller revolution. The suction side loading history (four harmonics) from the leading edge to the trailing edge is shown in Fig. 6. The pressure side loading history is shown in Fig. 7. One significant feature of these data is that there is an obvious phase shift in the unsteady pressure on the suction surface, whereas the phase angle is nearly constant on the pressure side. This behavior is similar to that of a compressor observed

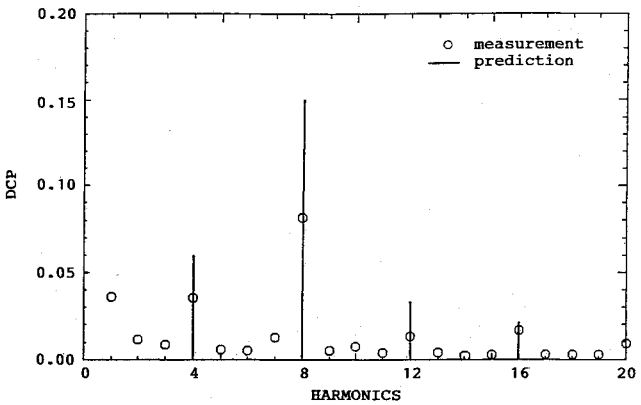

Fig. 10 Harmonic content of unsteady pressure on suction side.

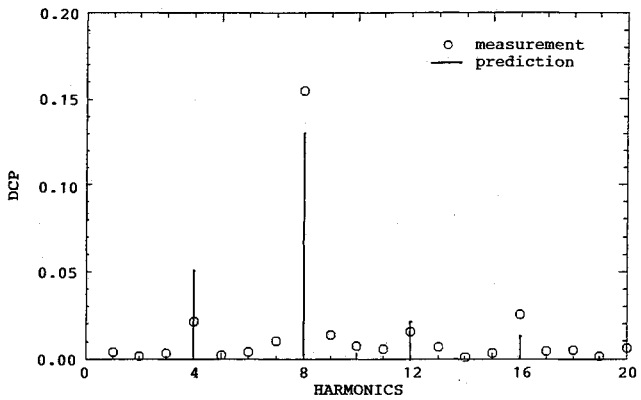

Fig. 11 Harmonic content of unsteady pressure on pressure side.

by Henderson and Franke.[15] The phase shifts indicate that the second harmonic (8 per rev) disturbance dominates the unsteady fluctuations. That is, the first order wake effect from the upstream impeller is the dominant excitation force to diffuser blades. The phase angle on suction and pressure surfaces are found to be in phase near the trailing edge. Thus, for a loaded trailing edge, the pressure difference across the blade trailing edge is zero.

Figures 8 and 9 show the comparison between calculated and measured time-dependent unsteady pressure variations at about 10% chord on suction and pressure surfaces for a 360-deg impeller revolution. The periodic nature of this response, 8 per revolution response to the wakeflow, is clear. In addition, the amplitude of pressure fluctuation is in good agreement. The Fourier components of the response are shown in Figs. 10 and 11 for suction and pressure surfaces respectively. The dominant frequency is the 8 per revolution impeller blade passing frequency. The multiples of the blade passing frequency decay rapidly. The second largest amplitude is the 4 per revolution. This indicates the loading on the full impeller blade is not quite the same as that on the partial blade. The decay characteristics of the unsteady response correlate well with the measurement despite the much higher 8 per revolution amplitude on the suction surface indicated by the predicted results. This may be attributed to the larger curvature and phase shift on the suction side compared with those on the pressure side, that a slight change on the phase of boundary condition may affect the prediction significantly.

The computation was performed on a DN4000 Apollo workstation, which is slower than most mainframe computers. However, as the analysis is performed in the frequency domain and interblade phase angles are used for periodic responses, only one blade (the reference blade) information is required for an unsteady cascade analysis, and the calculation is more efficient compared to other similar calculations. For a typical example shown in the paper (80 panels on each blade, 15 blades in cascade, and 100 wake panels), approximately 10 min of CPU is used for each individual frequency.

Conclusion

The purpose of this paper is to provide an improved and computationally efficient technique for investigating the dynamic loads caused by the interaction of a turbomachinery stage with the wakes of an upstream blade row. The method of analysis is basically for two-dimensional, inviscid, and incompressible flow. The method is incorporated with a Fourier analysis for nonsimple-harmonic unsteady flow. The application to the SSME HPOTP diffuser demonstrates the calculation. Because of the lack of experimental data, the present study can be viewed only as a simulation of the unsteady pressure fluctuation due to a blade-wake interaction. Nevertheless, the comparison between the predicted and several other measurements[12–15] does show that the amplitude of pressure fluctuation, wave propagation characteristics and frequency contents can be simulated well by using the present frequency domain method.

In general, the high frequency, as well as low frequency can be valid for the analysis, though the accuracy is limited to the grid size used. In addition, the use of interblade phase angles in frequency domain calculation, arbitrary wavelength excitation can be simulated.

In the present frequency domain method, a linear gust convection model is used. Although this model may not be able to trace the vortical flow exactly, the impact on the solution should be small as long as there is no significant in-passage vortical flow distortion or surface separation.

It should be noted that by using input velocities measured during turbopump operation, the velocities include any interaction effects between the rotating and stationary components. As seen from the example, with this velocity as an input, the resulting unsteady pressures on the downstream blade row do match the measured unsteady pressures very well, thus, any interactions are apparently accounted for, at least in their first order effects. Of course, during the design process, these measured velocities are not available. Any reasonable wake model given by Lakshminarayana and Davino,[16] Lefcort[17] or other gust velocity fields, can be used as stated in Chen.[10]

References

[1]Smith, S. N., "Discrete Frequency Sound Generation in Axial Flow Turbomachines," Ames Research Center (NASA); British Aeronautical Research Council RM 3709, 1971.

[2]Fleeter, S., "Fluctuating Lift and Moment Coefficients for Cascaded Airfoils in Nonuniform Compressible Flows," *Journal of Aircraft*, Vol. 10, No. 2, 1973, pp. 93–98.

[3]Henderson, R. E., "The Influence of Unsteady Rotor Response on a Distorted Flow Field," *Journal of Engineering for Power*, July 1982, Vol. 104, pp. 683–691.

[4]Rai, M. M., "Navier-Stokes Simulations of Rotor-Stator Interaction Using Patched and Overlain Grids," AIAA Paper 85-1519.

[5]Jorgenson, P. C. E., and Chima, R. V., "An Explicit Runge-Kutta Method for Unsteady Rotor/Stator Interaction," AIAA Paper 88-0049, 26th AIAA Aerospace Sciences Meeting, Reno, NV, 1988.

[6]Chen, Y. S., "3-D Stator-Rotor Interaction of the SSME," AIAA Paper 88-3095, 24th AIAA/ASME/SAE/ASEE Joint Propulsion Conference, Boston, MA, 1988.

[7]Celestina, M. L., Mulac, R. A., and Adamczyk, J. J., "A Numerical Simulation of the Inviscid Flow Through a Counter-Rotating Propeller," ASME Paper 86-GT-138.

[8]Morino, L., "A General Theory of Unsteady Compressible Potential Aerodynamics," NASA CR-2464, 1974.

[9]Chen, S. H., "Turbomachinery Blade Loading Prediction Using the Panel Method," *Second International Symposium on Boundary Element Methods*, East Hartford, CT, Oct., 1989.

[10]Chen, S. H., and Eastland, A. H., "Forced Response on Turbomachinery Blades Due to Passing Wakes," AIAA Paper 90-2353, 26th Joint Propulsion Conf., Florida, 1990.

[11]Rojas, L., "Test Report SSME High Pressure Oxidizer Turbopump Impeller Discharge Flow Dynamic Hot Wire Measurement,"

Rocketdyne Rept. R/H7173-5027, Jan. 1987.

[12]Mertesdorf, S., "Test Report: SSME High Pressure Oxidizer Turbopump Diffuser Vanes Dynamic Load Investigation," Rocketdyne Rept. R/H7173-5028, Jan. 1987.

[13]Arndt, N., Acosta, A. J., Brennen, C. E., and Caughey, T. K., "Rotor-Stator Interaction in a Diffuser Pump," *Journal of Turbomachinery*, Vol. 111, July 1989, pp. 213–221.

[14]Dring, R. P., Joslyn, H. P., Hardin, L. W., and Wagner, J. H., "Turbine Rotor-Stator Interaction," *Journal of Engineering for Power*, Vol. 104, No. 10, 1982, pp. 729–742.

[15]Henderson, R. E., and Franke, G., "Investigation of the Unsteady Pressure Distribution on the Blades of an Axial Flow Fan," NASA TM78-54.

[16]Lakshminarayana, B., and Davino, R., "Mean Velocity and Decay Characteristics of the Guidevane and Stator Blade Wake of an Axial Flow Compressor," *Journal of Engineering for Power*, Vol. 102, No. 1, 1980, pp. 50–60.

[17]Lefcort, M. D., "An Investigation into Unsteady Blade Forces in Turbomachines," *Journal of Engineering for Power*, Oct. 1965, pp. 345–354.